Transketolase is involved in the control of Sigma B during chronic infection by *Staphylococcus aureus*

Xin Tan[1,2], Elodie Ramond[1,2], Anne Jamet[1,2], Baptiste Decaux-Tramoni[1,2], Marion Dupuis[1,2], Daniel Euphrasie[1,2], Fabiola Tros[1,2], Ivan Nemazanyy[1,2,3], Jason Ziveri[1,2], Xavier Nassif[1,2], Alain Charbit[1,2] * and Mathieu Coureuil[1,2] *

[1] Université Paris Descartes, Sorbonne Paris Cité, Bâtiment Leriche, Paris, France

[2] INSERM U1151 - CNRS UMR 8253, Institut Necker-Enfants Malades, Paris, France

[3] Plateforme Métabolomique Institut Necker, Structure Fédérative de Recherche SFR Necker, Université Paris Descartes, Paris 75015 France

Running title: Transketolase in *S. aureus* intracellular persistence

Keywords: Transketolase, *Staphylococcus aureus*, metabolic adaptation, Pentose Phosphate Pathway, sigma B, intracellular persistence.

Bâtiment Leriche. 14 Rue Maria Helena Vieira Da Silva CS 61431 - 75993 PARIS – FRANCE

* Corresponding authors: Alain Charbit, Mathieu Coureuil

e-mail: alain.charbit@inserm.fr ; mathieu.coureuil@inserm.fr

Tel: 33 1 – 72 60 65 11 — Fax: 33 1 - 72 60 65 13

Abstract

Staphylococcus aureus is a leading cause of both acute and chronic infections in humans. Its ability to persist within host cells is thought to play an important role in chronicity and treatment failures. The importance of the pentose phosphate pathway (PPP) during *S. aureus* chronic infection is currently largely unexplored. Here, we focused on one key PPP enzyme, transketolase. We showed that inactivation of the unique gene encoding transketolase activity in *S. aureus* USA300 (Δ*tkt*) led to an impaired growth in broth. Using time-lapse video imaging, we correlated this phenotype with a defect in early intracellular proliferation compared to wild-type strain. As determined by metabolomic analysis, *tkt* inactivation also had an important impact on *S. aureus* metabolism. We then monitored long-term intracellular persistence over 10 days by counting of viable bacteria. Unexpectedly for such a slow-growing strain, the Δ*tkt* mutant was almost completely eliminated by endothelial cells after ten days, as opposed to a prototypical slow-growing Δ*hemDBL* mutant for which we recovered 1,000 fold more viable bacteria. We found that in infected cells, the transcriptional activity of the two master regulators Sigma B and RpiRc was drastically reduced in the Δ*tkt* mutant compared to wild-type strain. Concomitantly, RNAIII transcription was strongly increased. This transcriptional profile is likely to explain the inability of this slow-growing mutant to sustain long-term intracellular survival, suggesting that TKT -or a functional PPP- is required for intracellular bacteria to enable a transcriptional program geared towards persistence.

Importance

Staphylococcus aureus is a leading cause of severe bacterial infections. This bacterium is readily internalized by non-professional phagocytes and infected cells have been proposed to play an important role in chronic infections and treatment failures.

Here, we show the importance of the unique transketolase TKT of *S. aureus* USA300 in bacterial adaptation during chronic intracellular infection. We show that TKT is mandatory for the metabolomic homeostasis of *S. aureus* during intracellular persistence. This work unravels the critical role of TKT in the transcriptional regulation of the master regulators Sigma B, RpiRc and RNAIII linking the pentose phosphate pathway to the control of chronic *S. aureus* infections.

Introduction

Staphylococcus aureus is a Gram-positive bacterium that asymptomatically colonizes multiple anatomical sites including nares, respiratory tract and skin. *S. aureus* is also associated with severe skin and soft tissue infections, pneumonia, endocarditis and bone and joint infections (1, 2). In the last two decades multidrug resistant *S. aureus* appeared in the United States and Europe and dramatically complicates infection treatment, eventually leading to fatal outcomes (3). In particular, *S. aureus* USA300, an epidemic community-associated methicillin-resistant strain (CA-MRSA), has now emerged as the predominant cause of methicillin-resistant *S. aureus* (MRSA) infections in the United States and is continuously spreading around the world (4, 5).

After an acute inflammatory phase, *S. aureus* infections can become chronic due to inefficacy of the antibiotic treatment and/or impaired elimination by the host. The presence of persister bacteria is thought to play an important role in the relapse or the resistance of these chronic infections (6). The molecular bases of *S. aureus* persistence have been studied over the past two decades, and several regulatory circuits and metabolic pathways have been identified (7, 8). One phenotype of bacteria, designated “small colony variants” (SCVs) (9), has been particularly used as a model to study persistence. SCVs are defined by a reduced metabolic activity and a slow growth rate resulting in small-sized colonies on agar plates (10-12), The two most prevalent SCV phenotypes are characterized by deficiencies in the electron transport chain (menadione and/or hemin autotrophic SCVs) or in the thymidylate biosynthetic pathway (thymidine auxotrophic SCVs with *thyA* mutation) (13-16). These two families of SCVs both induce a decreased tricarboxylic acid (TCA) cycle activity and consequently lead to a down-regulation of the electron transport chain activity. It was notably found that *thyA* mutation was associated with decreased aconitase (CitB) abundance (13).

Interestingly, SCVs have the capacity to infect and survive within a wide range of eukaryotic host cells both *in vitro* and *in vivo* (9, 10, 17-24), possibly contributing to the long-term persistence of *S. aureus* in the airways of patients with chronic lung diseases despite appropriate antimicrobial treatments (25, 26). Intracellular *S. aureus* have evolved different

strategies to evade host defence machineries and silently persist within their intracellular location (27, 28). For instance, *S. aureus* can dynamically switch phenotypes from a highly aggressive and cytotoxic phenotype to a metabolically inactive phenotype associated with decrease TCA activity (15, 29-31). Reprogramming of the TCA cycle notably involves the glycolysis/gluconeogenesis and pentose phosphate pathway (PPP) (32). The contribution of glycolysis/gluconeogenesis to intracellular persistence of *S. aureus* has been already studied in some detail (33-36). In contrast, the precise role of the PPP is still largely unexplored.

The PPP is important for producing nucleotide precursors for DNA synthesis and repair as well as precursors for aromatic amino acids or peptidoglycan synthesis. In addition, the oxidative branch of the PPP contributes to bacterial tolerance to oxidative stress by generating the redox molecule NADPH,H^+, which is the substrate for other reducing agents such as glutathione. The activity of the PPP has been shown to be frequently increased in Gram-positive pathogens in response to environmental stresses and in infection models (37-39) or in some hospital-acquired isolates (40). While it has been suggested that the transcriptional regulator RpiRc might control the PPP (41-43), no gene regulation has been yet associated with any change in its activity in *S. aureus*.

Here, we study the role of PPP during the intracellular persistence of *S. aureus* by focusing on one of the key enzyme of this pathway, transketolase, a widely expressed enzyme in a wide range of organisms including bacteria, plants, and mammals, whose three dimensional crystallographic structure has been solved in several species (44, 45). We show that inactivation of the gene *tkt,* encoding the unique transketolase of *S. aureus* USA300, leads to significant decrease in intracellular bacteria proliferation and survival in endothelial cells, associated with a non-persister like phenotype, despite some SCV characteristics. Importantly, our data suggest a major role of the PPP in the control of the chronic stage of *S. aureus* intracellular survival.

Results

Transketolase inactivation in *S. aureus* USA300

S. aureus genomes possess a unique transketolase-encoding gene, designated *tkt*. The transketolase (TKT) protein of *S. aureus* USA300 (SAUSA300_1239) is 625 amino acid long and it shares 60.64%, 44.89% and 43.32% amino acid identity with the transketolases of *Bacillus anthracis*, *Francisella novicida* and *Mycobacterium tuberculosis*, respectively. This enzyme of the non-oxidative branch of the PPP is involved in two main reversible enzymatic reactions: i) Fructose-6-P + Glyceraldehyde-3-P <-> Erythrose-4-P + Xylulose-5-P; and ii) Sedoheptulose-7-P + Glyceraldehyde-3-P <-> Ribose-5-P + Xylulose-5-P **(Figure S1A)**.

To address the role of PPP in *S. aureus* persistence*, w*e generated a TKT defective mutant (designated Δ*tkt*) by chromosomal deletion of the *tkt* gene in *S. aureus* strain USA300, and a complemented strain (designated Cp-*tkt*) by introducing a plasmid-encoded copy of the wild-type *tkt* allele preceded by its own promoter in the Δ*tkt* strain (see Materials and Methods). We confirmed *tkt* inactivation by PCR sequencing and by quantification of the transketolase activity in the wild type (WT) strain and its two derivates Δ*tkt* and Cp-*tkt* (**Fig S1B)**. As expected, TKT activity was dramatically reduced in the Δ*tkt* mutant strain compared to WT (6.37 vs 41.75 $U.\mu g^{-1}$, respectively) and TKT activity was restored in the complemented strain (67.53 $U.\mu g^{-1}$), demonstrating successful functional complementation.

We evaluated the impact of *tkt* inactivation on bacterial growth in complete BHI medium, Dulbecco's Modified Eagle Medium (DMEM) or in chemically defined medium (CDM) (46) supplemented with various carbon sources. In BHI and DMEM**,** the Δ*tkt* mutant showed only a slight growth decrease compared to the WT (**Fig. 1A**). In contrast, a severe growth defect of the Δ*tkt* mutant was observed in CDM supplemented with glucose (a glycolytic substrate), and a complete absence of growth was observed in CDM supplemented with either glycerol or ribose (gluconeogenic- and PPP-substrates, respectively) (**Fig. 1A**), supporting the critical role of TKT for growth in the absence of glycolytic substrates. Complementation of the Δ*tkt* mutant with the wild-type allele (in Cp-*tkt*) restored almost normal growth in all conditions tested.

We checked colony morphology of the Δ*tkt* and Cp-*tkt* strains on BHI agar plates after an overnight culture. The Δ*tkt* strain formed small colonies (10-fold smaller than those formed by the wild-type strain) that are reminiscent of the small colonies formed by the hemin autotrophic strain Δ*hemDBL* (18) used here as a prototypical strain of SCV (**Fig. 1B**). The complemented strain showed partial phenotypic complementation with intermediate colony morphology (**Fig. 1B**).

We next evaluated the global impact of *tkt* deletion on bacterial metabolism. For this, we performed a whole cell metabolomic analysis on WT and Δ*tkt* strains grown for 24h in BHI Broth (*i.e.,* when identical numbers of cells were recorded) (**Fig. S1C-E and Table S2**). Remarkably, we observed a massive accumulation of ribose-5-phosphate (R5P; 56-fold increase) concomitant with a decrease in ribose content (4-fold decrease) in the Δ*tkt* mutant compared to WT. This accumulation was associated with an increased amount of metabolites derived from Ribose-5P, such as inosine-5-monophosphate (IMP), xanthosine-5-monophosphate (XMP) and hypoxanthine. We also observed a 2.5-fold decrease in D-sedo-heptulose-7P amount in the Δ*tkt* mutant compared to WT accompanied by a significant decrease in tyrosine, histidine and tryptophan amounts (5, 10 and 12 fold respectively), three aromatic amino-acids produced from the PPP. The glutamate pathway seemed to be significantly more active in the Δ*tkt* strain compared to WT as the amounts of glutamate, proline and ornithine were all increased. The higher amounts of glutamate, possibly fuelling the TCA cycle at the level of α-ketoglutarate, could be responsible for the increased expression of some TCA cycle metabolites (*i.e.,* fumarate, malate, succinate and α-ketoglutarate) in the Δ*tkt* strain. Of note, ATP content was not altered in Δ*tkt* strain.

These results demonstrated the drastic effect of *tkt* inactivation on PPP activity and more generally on the whole metabolism of *S. aureus* that may explain the slow-growth phenotype of the Δ*tkt* mutant strain.

***tkt* inactivation triggers a slow-growth but non-persister phenotype in infected endothelial cells**

One striking phenotype often reported for slow growing *S. aureus* strains is their ability to inhibit their proliferation inside infected host cells, allowing them to persist intracellularly for several days (15, 18, 19, 30, 31). This prompted us to follow the fate of WT and Δ*tkt* strains after entry into EA.hy926 endothelial cells by using: i) time lapse-microscopy, to evaluate early intracellular proliferation of *S. aureus* (18); and ii) colony forming units counting, to monitor the survival kinetics of internalized bacteria over a ten days period. The Δ*hemDBL* derivative strain was used as a prototype of a slow growing strain.

Study of intracellular S. aureus during the first 24 hours of infection by time-lapse video microscopy. We first generated cells with red nuclei by transducing EA.hy926 cells with NucLight Red Lentivirus to facilitate cell recognition and counting (see Materials and Methods for details). These cells were infected by GFP-expressing bacteria for one hour and extracellular bacteria were removed by the addition of gentamicin in the cell culture medium followed by several washes. Then, gentamicin was present throughout the experiment to prevent extracellular bacterial growth and re-infection. This procedure allowed us to focus only on the fate of intracellular bacteria. Images were captured every 30 minutes. Bacterial entry into endothelial cells was similar for WT, Δ*tkt* and Δ*hemDBL* strains, showing 0.3~0.5 GFP expressing particles recorded per cell (**Fig. 2A-B**). Active proliferation of WT *S. aureus* was confirmed after 24 hours of infection (**Fig. 2A-B and Video S1)** with an average number of GFP expressing particles rising from 0.5 to 2 per cells. At the single cell level, WT *S. aureus* showed active intracellular multiplication, ultimately leading to cell death and bacterial release in the extracellular medium (**Fig. 2A-B and Video S1**). Importantly, bacterial release did not lead to proliferation in the extracellular medium in our setting, because of the permanent presence of gentamicin in the medium. In contrast, the Δ*tkt* mutant strain showed limited proliferation during the first 24 hours alike the Δ*hemDBL* mutant (**Fig. 2A-B and Video S2, S3**). Finally, using LAMP-1 colocalization assay (Lysosome-associated membrane proteins 1) on infected cells, we confirmed that the low proliferation observed with Δ*tkt* strain was not due to a decreased phagosomal escape (**Fig. S2A**). LAMP-1 staining was performed on infected cells fixed at 1h or 24h after infection. Colocalization of LAMP-1 with WT or Δ*tkt* bacteria was of 56.4% and 55.4% at 1h, respectively, and went down to 26.3%

and 30% at 24h, respectively, indicating that phagosomal escape had occurred with both wild-type and Δ*tkt* mutant strains (**Fig. S2A**). Thus, time-lapse video microscopy of the first 24 hours of infection demonstrated that *tkt* inactivation resulted in an impaired early intracellular proliferation compared to WT strain.

Study of long-term intracellular survival over 10 days of infection by colony forming units (CFU) counting. We then monitored the kinetics of intracellular survival of the Δ*tkt* mutant in these cells by plating lysed cells onto solid medium at different time points after infection and counting bacteria able to form colonies (CFU). We had previously demonstrated that the slow growing Δ*hemDBL* mutant strain had a higher capacity to survive inside EA.hy296 endothelial cell line than the wild type *S. aureus* USA300 (18). Therefore, we compared the ability of intracellular Δ*tkt* mutant to survive inside EA.hy296 cells to that of Δ*hemDBL* and WT strains, by counting the number of viable intracellular bacteria (*i.e.,* able to form colonies on solid medium) three, seven or ten days after infection. Cells were infected and treated as for time-lapse experiment described above. Somewhat unexpectedly for a slow-growing mutant, the Δ*tkt* strain behaved like the WT strain throughout the infection period, ultimately leading to its complete elimination after 10 days (**Fig. 2C**). In contrast, for the prototypical slow-growing Δ*hemDBL* mutant we recovered almost 1,000 CFUs at day ten (**Fig. 2C**).

Altogether these data indicate that *S. aureus* USA300 defective for TKT has an atypical slow-growth phenotype that does not sustain long-term survival inside cells. Slow-growing variants usually exhibited modifications in the expression of their master regulators, which explain their ability to survive silently during extended period of time. Hence, to explain the inability of the Δ*tkt* slow-growing strain to persist intracellularly, we decided to study the transcriptional pattern of regulators known to be involved in persistence.

tkt inactivation is associated with and altered _rpiRc_ and _sigB_ expression.

S. aureus is known to sense its environment and to regulate virulence factors depending on the availability of substrates. For example, recent studies have shown that the transcriptional regulator RpiRc could sense metabolic shifts, especially in the PPP, and

control expression of RNAIII (41-43). RNAIII is a key effector in the quorum-sensing system that regulates the expression of a large number of virulence factors (47). RpiRc is also linked to the alternative Sigma B factor (SigB) that has pleiotropic roles in gene regulation and is a master regulator of intracellular persistence (7, 31, 42, 48). Of note, the activity of the *agr* system is repressed in SCVs and SigB has been shown to have a central role in the pathogenesis of SCVs (49).

These data prompted us to follow the expression profile of *sigB* and *rpiRc* in the WT and the Δ*tkt* mutant strains during long-term persistence within endothelial cells (**Fig. 3**). EA.hy296 cells were infected as for CFUs experiment described above to solely focus on intracellular bacteria. Between day 1 and day 7, *sigB* and *rpiRc* transcription increased in the WT strain (by 4-fold and 3-fold, respectively) (**Fig 3**). In sharp contrast, as early as one day after infection, both genes were significantly down-regulated in the Δ*tkt* mutant strain compared to WT (8-fold and 7-fold decrease for *sigB* and *rpirC* expression, respectively). Consistent with reports demonstrating inhibition of RNAIII expression by RpirC and SigB (31), we observed a dramatic increase in the expression of *RNAIII* in the Δ*tkt* mutant strain (**Fig. 3**), suggesting that the Δ*tkt* mutant strain is unable to control *rpiRc* and *sigB* expression during prolonged intracellular survival. Importantly, this defect was not observed in the slow-growing strain Δ*hemDBL* (**Fig. S2B**), possibly accounting for the prolonged intracellular survival of this mutant. To further confirm these data, we monitored the expression of two major regulators of SigB activity, RsbU and RsbW (50). RsbW, which is co-expressed with SigB, is known to sequestrate and inhibit SigB. RsbU, whose expression is under the control of SigA, is a phosphatase involved in the dephosphorylation of RsbV. In turn, dephosphorylated RsbV (dRsbV) is able to sequestrate RsbW, allowing the release of active SigB. RsbU is thus considered as an activator of SigB, allowing a fine tuning of SigB activity.

We found that the transcription of both *rsbW* and *rsbU* genes was down-regulated in the Δ*tkt* mutant during infection of endothelial cells. The down-regulation of *rsbW* is consistent with the down-regulation of its co-expressed gene *sigB* (**Fig. 3**). The concomitant down-regulation of *rsbU* suggests a global inhibition of the *sigB* pathway in the Δ*tkt* mutant strain. Finally, we followed expression of *asp23,* a *sigB*-dependent locus (51, 52). The recorded down-

regulation of *asp23* transcription in the Δ*tkt* mutant strain confirmed the inhibition of SigB-dependent transcription.

Altogether these transcriptional analyses suggest that TKT -or a functional PPP- is required for the bacteria to enable a transcription program geared towards intracellular survival.

The SigB pathway may be controlled by modulating carbon source availability.

The above results suggested that the PPP might take control of *rpiRc* and *sigB* expression when bacteria persist in endothelial cells. We thus hypothesized that PPP-associated carbon sources may possibly influence *rpiRc* and/or *sigB* expression *in vitro*. We therefore grew WT USA300 in CDM supplemented either with glucose, ribose (one product of PPP, **Fig. 1**) or fructose (a carbon source possibly fuelling the PPP, **Fig. S3**) and quantified by qRT-PCR transcription of *sigB*, *rpiRc*, *rsbU/W* and *asp23* genes. Remarkably, we found that the regulation of the whole *sigB* operon was impacted by the carbon source used in CDM (**Fig. 4**). Indeed, the expression of *sigB, rsbU/W* and *rpiRc* decreased in CDM supplemented with either fructose or ribose, compared to CDM supplemented with glucose. In contrast, *asp23* expression was only decrease by 2-fold in CDM supplemented with fructose and increased by 3-fold in CDM supplemented with ribose, suggesting that in this growth conditions, *asp23* expression might be regulated by other factor than *sigB* (**Fig. 4**). Hence, the availability of carbon sources, and especially those related to PPP, may be sensed by the bacteria and affect the regulation of *rpiRc* and *sigB* expression.

Bioavailability of PPP carbon sources impacts intracellular growth of *S. aureus* independently of SigB.

We then reasoned that the modification of carbon source concentration in endothelial cells might also alter initial proliferation and long-term persistence of bacteria within host cells. We therefore followed growth and persistence of intracellular WT USA300 in endothelial cells cultured in no glucose DMEM supplemented with either glucose or fructose or ribose (25 mM each). First, using time-lapse microscopy we focused on intracellular proliferation during the first day after infection. We observed a drastic inhibition of intracellular WT proliferation

during the first 24h after infection when cells were grown in DMEM supplemented with fructose or ribose compared to DMEM supplemented with glucose (**Fig. 5A and video S4, S5**). Indeed, while WT USA300 grew up to 3~4 bacteria per cell in DMEM supplemented with glucose, the number of bacteria per cell remained around 1 in DMEM supplemented with ribose or fructose. Then, we focused on later stages of infection by CFU counting at day 3 and day 7 post-infection. Survival of intracellular bacteria was only very modestly impaired in ribose or fructose (with only a slight but significant 5- to 6-fold decrease in the number of CFUs) (**Fig. 5B**).

We next monitored *sigB*, *rsbU/W* and *asp23* expression during intracellular persistence of WT USA300 in these different cell culture conditions (**Fig. 5C**). No relevant difference in *sigB* expression was recorded between the three cell growth conditions. Growth of WT USA300 in DMEM supplemented with ribose was associated with a reduced expression of *rsbU* throughout the infection period and with that of *rsbW* only at day 3. Expression of *asp23* was increased by less than 2-fold in cells grown with fructose or ribose after the three first days of infection. These results, which are not consistent with the expression profiles observed in CDM, may be explained by the fact that the intracellular pools of fructose, ribose and glucose available to intracellular *S. aureus* had not been sufficiently modified in the experimental conditions tested. To test this possibly, we compared the metabolomic profile of non-infected cells cultivated for 1, 3 or 7 days with DMEM supplemented with either glucose or fructose or ribose (**Fig. S3 and Table S2**).

As expected, cells grown in the presence of fructose and ribose had a significant reduction of their intracellular glucose pool (more than 500-fold decrease in relative concentration) compared to those grown in the presence of glucose. Somewhat unexpectedly, the relative concentration of fructose was 10-fold higher in glucose-treated cells than that in fructose-treated cells. In ribose-grown cells, the relative concentrations of ribose and sedoheptulose were higher than with the two other carbons sources at all time points (a 1,000-fold increase in ribose concentration was recorded). However, the relative concentration of R5P was not different between the three conditions tested. Otherwise, no major variation in the intracellular metabolome was observed with the three different carbon sources.

Discussion

We showed here that inactivation of the unique gene *tkt*, encoding transketolase in *S. aureus* USA300, conferred a slow-growth phenotype and was associated with important metabolomic alterations during planktonic growth. In infected cells, *tkt* inactivation also decreased bacterial intracellular persistence, most likely because of a drastic reduction of transcription of Sigma B- and RpiRc-encoding genes. Altogether our data highlight a novel connection between the PPP and these master regulators controlling chronic bacterial intracellular persistence.

S. aureus SCVs have been particularly used as a model to study persistence (9, 17, 18, 20, 53-56). As recalled earlier, the SCV phenotype is generally associated with the formation of tiny colonies on plates, increased biofilm capacity and antibiotic resistance. Furthermore, supernatants from SCVs cultures generally show reduced cytotoxicity on cell cultures. The Δ*tkt* mutant of *S. aureus* USA300 shared the common properties of SCVs in planktonic conditions. The behaviour of the Δ*tkt* mutant of *S. aureus* USA300 was also similar to a slow-growing strain (here Δ*hemDBL*) in time-lapse video microscopy, at the single cell level over a 24 hours-period. Somewhat unexpectedly, bacterial counts revealed that after seven days, the wild-type strain and the Δ*tkt* mutant showed similar intracellular survival decrease, ultimately leading to their complete elimination whereas the Δ*hemDBL* strain was still clearly detected even after ten days inside cells. Confocal microscopy analyses did not reveal any phagosomal escape defect of the Δ*tkt* mutant. To study the survival of wild-type and Δtkt mutant strains inside endothelial cells, we followed two complementary approaches. While time-lapse microscopy experiments allowed us to evaluate the ability of newly internalized bacteria to grow and proliferate inside cells during the first 24 hours after infection (*i.e.* early proliferation), we could follow the survival of low-proliferative intracellular persisters up to 10 days after infection by counting CFUs. These complementary approaches defined the Δ*tkt* mutant as a non-proliferative and non-persister strain. Among the most striking transcriptional changes recorded in the Δ*tkt* mutant compared to WT *S. aureus* USA300, was an increase in RNAIII transcription at day 1 and

day 3 in infected cells. Simultaneously, the Δ*tkt* mutant showed a severe decreased transcription of *rpiRc* and *sigB* genes. In general very low levels of RNAIII, either due to an inactivated *agrBDCA* operon or to an increased RNAIII degradation, constitute a hallmark of electron transport chain related SCVs (29, 57-59). The *agr* system constitutes one of the major and best-characterized players in *S. aureus* intracellular survival. Indeed, the up-regulation of the *agr* locus, that triggers the expression of secreted virulence factors such as hemolysins and leukocidins, is unfavourable for intracellular persistence (10). RpiRc, one of the three members of the transcriptional regulator RpiR family controlling enzymes involved in sugar catabolism in *S. aureus*, appears to function as a metabolite-responsive modulator of the *agr* system, that also negatively-controls RNAIII transcription (43). Of note, RpiRc has been shown to repress RNAIII (41), supporting the notion of a direct connection between the PPP and the regulation of *S. aureus* virulence. The expression of SigB has also been shown to play a crucial role during persistence possibly by down-regulating pro-inflammatory virulence factors and increasing the expression of factors promoting persistence (7) and *sigB* mutants are completely cleared by the host cells and fail to form SCVs (31). TKT inactivation which triggers the up-regulation of RNAIII and down-regulation of *sigB* and *rpiRc* appears thus to confer a non-persister phenotype during chronic infection of host cells.

A number of "Omics" approaches have been carried out to explain why *S. aureus* SCVs have a reduced metabolic activity and how these metabolic changes affect persistence (29, 60, 61). During its intracellular survival, a *Δtkt* mutant is likely to deal simultaneously with PPP blocking and altered levels of carbon-based nutrients. Our whole cell metabolomic analysis of planktonic-grown bacteria (**Fig. S1C-E and Table S2**) showed a huge increase in R5P intermediates in the Δ*tkt* mutant compared to wild-type that could be explained by the impaired entry of R5P into glycolysis and a concomitant significant decrease in SH7P relative concentration. We also observed significant changes in the relative concentrations of TCA cycle intermediates and TCA-related amino acids compared to WT strain. For example, we observed a decrease in citrate and cis-aconitase amounts, corresponding to the very first TCA intermediates, in Δ*tkt* mutant compared to wild-type, which would account for a limited fuelling of the TCA cycle at this stage. In contrast, we noted a significant increase in the

relative concentrations of following TCA cycle intermediates such as α-ketoglutarate, succinate, fumarate and malate in Δ*tkt* mutant that could be due to an increased import of proline and glutamine (**Fig. S1C-E**). The TCA cycle plays a central role in maintaining the bacterial metabolic status and has been repeatedly implicated in the regulation of staphylococcal virulence (62-64). Activity of TCA cycle enzymes, the amounts of biosynthetic intermediates and generated ATP can be affected by a number of conditions, including: i) nutrients availability, ii) a stressful environment (*e.g.,* an intracellular environment), or iii) stress-inducing stimuli that alter carbon flux or here the PPP. These changes induce alterations of the overall metabolome of the bacterium that, in turn, may modulate the activity of metabolite-responsive global regulators such as SigB or RpiR.

We found that bacteria grown in CDM supplemented with ribose or fructose had reduced *sigB* expression during stationary phase. We thus hypothesized that the modification of carbon source availability inside infected cells might be a suitable strategy to act on *sigB* expression and therefore impair *S. aureus* intracellular persistence. We were not able to modify sufficiently the carbon source availability in the cytoplasm of infected endothelial cell, using DMEM supplementation with either ribose or fructose, to abrogate *S. aureus* USA300 intracellular persistence. A modest reduction of *S. aureus* intracellular persistence was however recorded with both sugars. At any rate, impaired bacterial intracellular survival might also be due to a global modification of the endothelial cell physiology. For instance, fructose uptake by cells may be linked to oxidative stress, inflammation and autophagy (65) (66). Other carbon sources, non-toxic to the cell and with better efficacy on *S. aureus* intracellular survival control, could be the focus of future research.

We propose the following model (**Fig. 6**) to try to integrate the data obtained in this work on *S. aureus* intracellular persistence and the current abundant literature on *S. aureus* regulatory circuits. In wild-type *S. aureus*, transketolase activity results in a positive regulation of *rpiRc* and *sigB* transcription and allows the repression of RNAIII. Consequently, repression of toxins production favours intracellular persistence. In contrast, in a Δ*tkt* mutant,

rpiRc and *sigB* transcriptions are not activated, possibly due to metabolic changes (such as R5P accumulation) and RNAIII is not repressed. At this stage, it cannot be excluded that the enzyme itself might also directly affect transcription of these regulators.

Ribose is present in the 100 µM range in human blood (67) and R5P concentration inside human lymphoblast is 70 µM (68)**.** It is thus likely that the availability of ribose in the tissues may directly affects *S. aureus* pathogenesis by influencing bacterial growth. Interestingly, *S. aureus* grown in CDM supplemented with ribose showed a decreased expression of *sigB*. In *S. aureus*, ribose is likely imported by the RbsU transporter and converted to R5P by the RbsD/RbsK pathway. R5P either becomes part of the PPP or serves as the precursor for nucleotide synthesis. Of note, RbsR (a repressor of *rbsUDK* operon) is itself highly regulated by SigB (69). Hence, stress signals that modulate SigB activity are likely to be important effectors for controlling the quantity of RbsR, thereby affecting ribose uptake.

The present work highlights an unprecedentedly reported role of transketolase in *S. aureus* intracellular persistence. Modulation of the pentose phosphate pathway activity may represent an interesting mean to impair *S. aureus* survival during chronic infections.

Materials and Methods

Strains, Cells, Culture conditions and Infection.

S. aureus. The epidemic clone *S. aureus* USA300-LAC (designated USA300-WT) was provided by the Biodefense and Emerging Infections Research Resources (BEI). The GFP-expressing strain was generated by curing the p03 plasmid from USA300-WT and introducing the pCN57-GFP recombinant plasmid (obtained from the BEI) by electroporation as described before (18). The Δ*hemDBL* derivative was constructed using the pMAD-temperature-sensitive shuttle vector system and was described before (18). The Δ*tkt* mutant strain and the complemented strain were constructed as described below. Strains and plasmids used are summarized in table S1A.

Before experiments bacteria were grown 24 hours at 37°C on BHI agar plates supplemented with antibiotics when required and then overnight in BHI Broth from an optical density 600 nm (OD_{600}) of 0.05. The day of experiment, bacteria were resuspended in BHI broth to an OD_{600} of 0.05 and grown at 37°C until the culture reached the initial-middle log phase (OD_{600} of 0.6).

Growth curve were performed in brain heart infusion, DMEM and chemically defined medium (CDM) supplemented with ribose or fructose or glycerol when it was required (46).

Internalization rate and survival inside the EA.hy926 endothelial cell line were similar between the GFP strain and the parental strain.

Cell line. EA.hy926 cell line (ATCC CRL-2922), originally derived from human umbilical vein, were grown in Dulbecco's modified Eagle high glucose medium (DMEM, Dominique Dutscher) supplemented with 10 % fetal bovine serum (FBS, Thermofisher scientific) in a humidified 5 % CO_2 atmosphere at 37 °C. When indicated cells were incubated with no glucose DMEM supplemented with glucose, ribose or fructose at a concentration of 25mM. To facilitate cell identification and counting during time lapse experiments, EA.hy926 cells were transduced with the IncuCyte® NucLight Red Lentivirus, following the manufacturer's

recommendations, to obtain red nuclear labelling of living cells due to the expression of the red fluorescent protein mKate2 containing a nuclear localization signal.

Infection.

When fresh cultures reached OD_{600} of 0.6, bacteria were added to endothelial cells at a multiplicity of infection (MOI) of 1 and placed in a humidified 5 % CO_2 atmosphere at 37 °C for 1 h. One hour after infection, each well was washed three times with 100 µL of phosphate buffer saline (PBS) containing 300 µg/mL gentamicin, to remove extracellular bacteria. Cells were then incubated with 100 µL of cell culture medium containing 50 $\mu g.mL^{-1}$ gentamicin. Infected cells were kept in a humidified 5 % CO_2 atmosphere at 37 °C. Importantly, gentamicin is an antibiotic with a high bactericidal effect on *S. aureus* USA300 (CMI=2 $\mu g.mL^{-1}$) and a very poor penetration inside eukaryotic cells. In our model the use of gentamicin in the extracellular medium was necessary to abolish extracellular proliferation.

Construction of the *S. aureus* Δ*tkt* chromosomal deletion mutant

We inactivated the *tkt* gene in wild-type *S. aureus* USA300 strain and substituted it by the kanamycin resistance gene *npt*II fused with pG*ro* promoter. For this, we used the pMAD-temperature-sensitive shuttle vector system (70). Briefly, the recombinant plasmid pMAD-Δ*tkt* was constructed by overlap PCR. First, the two regions (upstream 694bp, downstream 567bp) flanking *tkt* and the *npt*II gene (fused with pG*ro* promoter 1,091bp) were amplified by PCR. The region (2,352 bp) was then amplified by two-step overlap PCR. The resulting PCR product was cloned in pMiniT 2.0 (to yield recombinant plasmid pMiniT/tktUp-npt-tktDown). This recombinant plasmid was digested with *Bam*HI and *Eco*RI (New England BioLabs) and the *Bam*HI-*Eco*RI tktUp-npt-tktDown DNA fragment was finally subcloned into *Bam*HI-*Eco*RI-digested pMAD. All PCR reactions were realized using Phusion High-Fidelity DNA Polymerase (Thermofisher Scientific) and PCR products were purified using QIAquick PCR purification kit (Qiagen). The pMAD-Δ*tkt* plasmid was first introduced into *S. aureus* RN4220 prior to electroporation into *S. aureus* USA300. We used a standard two-step allelic exchange procedure (70) to create the chromosomal *S. aureus* USA300 Δ*tkt* strain. The Δ*tkt*

strain was finally checked for loss of the corresponding wild-type genes by PCR sequencing (Eurofins Genomics) using specific primers (Table S1B).

Construction of the complementation of *S. aureus* Cp-*tkt* strain

The plasmid pCN57-CP*tkt* was constructed by homologous recombination (71). The pCN57 linear vector and *tkt* gene fragments were amplified by PCR. To allow recombination, overlapping region of 20pb was added at each ends. PCN57 was linearized using SphI (New England BioLabs). *E. coli* DH5α were chemically transfected with a mix of both PCR product (insert: vector stoichiometry 2:1, 100ng of vector) in 10 µl MilliQ water. The colonies containing plasmid pCN57-CP-*tkt* were checked by PCR and the construct was sequenced. The pCN57-CP-*tkt* vector was then transfected into *S. aureus* RN4220 prior to electroporation into *S. aureus* USA300 Δ*tkt*. The Δ*tkt*-Cp-*tkt* (Cp-*tkt*) strain was finally checked for complementation of wild-type genes by PCR sequencing (Eurofins Genomics) using specific primers.

Time lapse microscopy

Four days prior to infection, NucLight Red labelled EA.hy926 cells were seeded in ImageLock 96-well plates (Essen BioScience Inc) in culture medium without antibiotic. Cells were infected with wild-type and mutant of the GFP-expressing USA300 strain as described above. Plates were incubated and monitored at 5% CO2 and 37°C for 24 hours in the fully automated microscope Incucyte® S3 (Essen BioScience). Images were taken every 30 minutes with the 20X objective. The medium was changed once during the observation period. Analysis and time-lapse videos (from which images were extracted) were generated by using Incucyte® S3 software.

Detailed analysis: Green items were analysed with a threshold of 1 GCU and using Top-hat segmentation mode. Red item were analysed with a threshold of 3 RCU and using Top-hat segmentation mode and edge sensitivity of -25. A spectral unmixing of 10% was applied to remove red signal from green signal. Green item counts were considered as an approximation of the number of intracellular bacteria, and red item counts considered as the

number of EA-hy296 cells. (Green items/Red items) represents the number of intracellular bacteria per cell during the time of infection.

Transcriptional analyses

Intracellular bacteria RNA extraction: EA.hy926 cells were grown to confluence in 75 cm^2 flasks and infected with *S. aureus* as described above. At selected time points, the culture medium was removed and the flasks were washed twice with PBS without antibiotics. Cells were lysed with 5 mL of distilled water for 10 min and the surface of the flask was scraped to detach the cells. The contents were recovered and centrifuged for 5 min at 3000 *g*. The supernatant was carefully removed and the pellet (which contained cell debris and bacteria) was resuspended in 100 µL of TE buffer containing 20 µg of lysostaphin and incubated for 5 minutes at 37 °C (72) to allow cell wall peptidoglycan degradation.

Planktonic bacteria RNA extraction: S. aureus was resuspended in CDM supplemented with glucose, ribose or fructose to an OD_{600} of 0.05 and grown overnight at 37°C. Bacteria were centrifuged at 12 000 *g* for 2 min and incubated in 50 µL of TE buffer containing 10 µg of lysostaphin for 5 minutes at 37 °C. The samples were resuspended in Trizol (Thermofisher Scientific) and treated with chloroform. RNAs were recovered using RNeasy Clean-up column (Qiagen) and DNA was digested using Turbo Dnase (Thermofisher Scientific). RNA concentration was measured using NanoDrop 1000 (Thermofisher Scientific). Reverse transcription was carried out with 500 ng of RNA and 0.5 µg of random primers (Promega). After denaturation at 70 °C for 5 min, 15 µL of the mix containing 4 µL M-MLV 5 X reaction buffer, 1 µL of 0.5 mM PCR Nucleotide Mix, 0.5 µL of RNasin Ribonuclease Inhibitor, and 1 µL M-MLV Reverse Transcriptase (Promega) was added. Samples were incubated 5 min at 25 °C, 1 h at 42 °C, then 15 min at 70 °C and chilled on ice. Quantitative RT-PCR was performed using FastStart SYBR Green qPCR Master Mix (ThermoFischer Scientific) or Luna Universal qPCR Master Mix (New England Biolabs) according to the manufacturer's recommendations. Transcript levels were analyzed using a 7900HT Fast Real-Time PCR System (Applied Biosystems) according to the standard settings of the system software. The thermal cycling conditions were: 50°C for 2 min, 95°C for 10 min, followed by 40 cycles of

95°C for 15 s and 60°C for 1 min. Gene specific primer sequences are presented in table S1B. Expression of the gene *gyrA* was chosen as a reference. We used the "The Relative Standard Curve Method" for analyzing the qRT-PCR data.

Metabolomic analyses

Bacteria: Metabolite profiling of *S. aureus* isolates was performed by liquid chromatography–mass spectrometry (LC-MS) as described (19, 73). Two independent experiments with three biological replicates were performed for each isolate. Briefly, *S. aureus* strains were grown in BHI Broth overnight to stationary phase and pelleted by centrifugation. Metabolic activity was blocked by immersion in liquid nitrogen for 10 sec. Metabolites were extracted using a solvent mixture of Methanol/ACN/H2O (50:30:20) at −20 °C (Extraction solution). Samples were vortexed for 5 min at 4°C, and then centrifuged at 16,000 g for 15 minutes at 4°C.

Endothelial cells: EA.hy926 endothelial cells were grown to confluence on a 12-well plate in no glucose DMEM supplemented with glucose or fructose or ribose (25 mM). One independent experiment with three biological replicates was performed for each condition. At each time points the cells were washed with cold PBS. Metabolism was blocked by plunging the plate into liquid nitrogen for 10 seconds. The cell metabolites were extracted from the samples by placing the cell culture plate on a rocking shaker at 4°C for 10 minutes. The extraction solution from each well was then collected and centrifuged at 16,000 g for 15 minutes at 4°C.

The supernatants were collected and analysed by LC-MS using SeQuant ZIC-pHilic column (Millipore) for the liquid chromatography separation (73). The aqueous mobile-phase solvent was 20 mM ammonium carbonate plus 0.1% ammonium hydroxide solution and the organic mobile phase was acetonitrile. The metabolites were separated over a linear gradient from 80% organic to 80% aqueous phase for 15 min. The column temperature was 48 °C and the flow rate was 200 µl/min. The metabolites were detected across a mass range of 75–1,000 m/z using the Q-Exactive Plus mass spectrometer (Thermo) at a resolution of 35,000 (at 200 m/z) with electrospray ionization and polarity switching mode. Lock masses were used to insure mass accuracy below 5 ppm. The peak areas of different metabolites were

determined using TraceFinder software (Thermo) using the exact mass of the singly charged ion and known retention time on the HPLC column. By this approach we were able to identify and measure: Glucose, Glucose-6P (G6P), UDP-glucose (UDP-Glc), Sedoheptulose-7-P (SH-7P), Ribose 5-phosphate, Glyceraldehyde 3-phosphate, Lactate, Pyruvate, Phospho-Enol-Pyruvate (PEP), Citrate (Cit), cis-aconitate (cis-aco), Succinate (Suc), Fumarate (Fum), Malate (Mal), alpha ketoglutarate (aKG), dihydroxyacetone phosphate (DHAP), N-carbamoyl-L-aspartate, Nicotinamide adenine dinucleotide (NAD), NADH, Nicotinamide adenine dinucleotide phosphate (NADP), NADPH, Adenine, Adenosine, Adenosine Mono, Di and Tri-phosphate (AMP, ADP, ATP), Cytidine, Cytidine Mono, Di and Tri-phosphate (CMP, CDP, CTP), Uridine Mono, Di and Tri-phosphate (UMP, UDP, UTP), Hypoxanthine, Guanine, Guanaosine, Guanidine Mono and Di-phosphate (GMP, GDP), Inosine monophosphate (IMP), Pantothenate, Dephospho-Coenzyme A, Coenzyme A (CoA), Flavin adenine dinucleotide (FAD), Niacin, Nicotinamide, 3-hydroxybutyrate, Urate, 5-oxo-L-Proline, Acetyl-aspartate, Acetyl-glutamine, Alanine, Arginine, Argininosuccinate, Asparagine, Aspartate, Betaine, Citrulline, Cystathionine, Cystine, Glutamine, Glutamate, Glycine, Histidine, IsoLeucine, Leicine, Sarcosine, Lysine, Methionine, Ornithine, Phenylalanine, Proline, Serine, Taurine, S-Adenosyl-L-methionine, Threonine, Tryptophan, Tyrosine, Valine, Butyric acid, Carnitine, Decanoic acid, Lauric acid, Hexanoic acid, Linoleic acid, Myristic acid, Octanoic acid, Oleic acid, Palmitic acid.

Statistical analyses were performed using MetaboAnalyst 4.0 software (74, 75). The algorithm for heatmap clustering was based on the Pearson distance measure for similarity and the Ward linkage method for biotype clustering. Metabolites with similar abundance patterns were positioned closer together.

Transketolase activity assay

Bacteria were grown to stationary phase in BHI Broth and 1 ml of culture was harvested. Bacteria were washed in PBS, pelleted by centrifugation, and resuspended in 300 µl of 50 mM Tris with 60 µg lysostaphin, pH 7.5. Samples were incubated at 37 °C for 5 min and then sonicated at 4 °C (30s on, 30s off, repeated 30 times) (Diagenode). Samples were

centrifuged at 12,000 *g* and 4 °C for 10 min to remove cell debris and protein concentration was determined using BCA assay with BSA as a standard (Thermo Fisher Scientific). TKT activity was analysed as described previously (76). Briefly, each enzymatic reactions were performed at a final volume of 100 µl containing 20 µl of supernatant, 50 mM Tris (pH 7.5), 0.24 mM $MgCl_2$, 10 µM thiamine pyrophosphate, 0.5 mM NADH, 3 units of glycerol-3-phosphate dehydrogenase, 10 units of triosephosphate isomerase, 0.5mM D-xylulose-5-phosphate, and 0.5mM D-erythrose-4-phosphate (all reagents obtained from Sigma-Aldrich). The reaction proceeded at 37 °C for 5 min, and the decrease in $A_{340\ nm}$ was monitored with a microplate reader (Molecular Devices). Transketolase enzyme activity in bacteria lysates was expressed as units per microgram of total protein. One unit of enzyme was defined as the amount of enzyme that oxidized 1 µmol of NADH per minute.

LAMP-1 colocalization assay

EA.hy926 endothelial cells were grown to confluence on 8-well Slides (Lab Tek II) and infected with *S. aureus* as described above. For each point, cells were washed 3 times with PBS and fixed 20 min in PBS-4% paraformaldehyde at 4 °C. Fixation was stopped in PBS-NH_4Cl 50 mM. Cells were permeabilized with PBS containing 0.1% saponin and 5% goat serum for 10 min on ice. Cells were incubated for 30 min with anti-LAMP-1 (Lysosomal-associated membrane protein 1) rabbit polyclonal antibody (1/200e, AbCam) diluted in PBS containing 5% goat serum (staining buffer). After washing, cells were incubated for 30 min with Alexa-568 conjugated donkey anti-rabbit secondary antibodies (1/400e, AbCam) diluted in staining buffer. After washing, 4,6-diamidino-2-phenylindole (DAPI) was added (1/10,000e) for 20 min and glass coverslips were mounted in Mowiol (Cityfluor Ltd.). Cells were examined using an X63 oil-immersion objective on an Apotome microscope (Zeiss™). Colocalization of GFP expressing bacteria with LAMP-1 staining was quantified by using Image J software (plug in: Coloc based Sur-vol _ Beta v6). Data were obtained from more than 200 infected cells for each condition and expressed as % of bacteria associated with LAMP-1 ± SD.

Statistics

Data were analyzed using GraphPad Prism software. Results are presented either with one representative experiment for clarity or as means ± standard deviation (SD). The number of biological and technical replicates is indicated in the legend of each figure. For two-sample comparisons statistical significance was measured using unpaired two-tail Student's t-test. For comparisons between more than two groups, statistical significance was measured using one-way analysis of variance (ANOVA) with Dunnett's correction. P values of $p<0.05$ were considered to indicate statistical significance.

Acknowledgements

Funding details. These studies were supported by INSERM, CNRS and Université Paris Descartes Paris Cité Sorbonne. Xin Tan was funded by a scholarship from the China Scholarship Council (n° CSC NO. 201508500097).

The funders had no role in study design, data collection and analysis, decision to publish, or preparation of the manuscript.

We are grateful to the Cell imaging core facility of the "Structure Fédérative de Recherche" Necker INSERM US24/CNRS UMS3633 for his technical support.

The following reagents were provided by the Network on Antimicrobial Resistance in *Staphylococcus aureus* (NARSA) for distribution by BEI Resources, NIAID, NIH: *Staphylococcus aureus*, Strain USA300-0114, NR-46070; *Escherichia coli – Staphylococcus aureus* Shuttle Vector pNR-46158, Recombinant in *Staphylococcus aureus*, NR-46158.

Legends

Figure 1. Phenotypic characterization of the Δ*tkt* mutant

A. Growth of USA300 wild type (WT), Δ*tkt* mutant (Δ*tkt*) and its complemented derivative (Cp-*tkt*). USA300 WT, Δ*tkt* and Cp-*tkt* strains were grown in BHI, DMEM or in chemically defined medium (CDM) supplemented with glucose, glycerol or ribose and incubated 21 hours at 37°C. Optic densities were measured every-hour from 0 to 8 hours and then at 21 hours. Each curve is a representative experiment.

B. Colony morphology. USA300 WT, Δ*tkt,* Cp-Δtkt and Δ*hemDBL* strains were grown on BHI agar plates for 24 hours at 37°C and colony morphology was imaged. Upper panel: plates. Lower panel: representative images. Bar = 1mm.

Figure 2. Intracellular proliferation and persistence of *S. aureus*.

A, B. Early intracellular proliferation of USA300 wild type (WT), Δ*tkt* mutant (Δ*tkt*) and Δ*hemDBL* mutant (Δ*hemDBL*) strains. Endothelial EA.Hy926 cells expressing a nuclear restricted Red Fluorescent Protein were infected with GFP expressing WT, Δ*tkt* and Δ*hemDBL* strains. One hour after infection cells were washed several times with gentamicin containing medium to eliminate extracellular bacteria. Gentamicin concentration of 50µg/ml was maintained throughout the experiment. Images were acquired every 30 minutes using Incucyte® S3 live cell imaging system. A. Representative images (see also video S1, S2 and S3). Red: cell nuclei. Green: GFP expressing bacteria. For each line, a white circle was centred on a unique infected cell. Bar = 100µm. B. Quantitative analysis representing the number of green particles divided by the number of red nuclei during the first day after infection.

C. Persistence of intracellular WT, Δ*tkt* Δ*hemDBL* strains. Endothelial EA.Hy926 cells were infected with WT, Δ*tkt* and Δ*hemDBL* strains as described above. Gentamicin was maintained throughout the experiment. Survival of *S. aureus* was assessed by plating and counting CFUs three, seven and ten days after infection. Results are shown as mean ± SD of triplicate measurements (ANOVA, ** $p<0.001$).

Figure 3. Transcription profile of intracellular *S. aureus*.

Endothelial EA.Hy926 cells were infected with USA300 WT and Δ*tkt* strain as described in figure 2. One, three or seven days after infection cells were washed and collected. RNA from intracellular *S. aureus* were prepared and gene expression of *RNAIII*, *rpiRc*, *sigB*, *rsbU, rsbW* and *asp23* was analysed by quantitative RT-PCR. Gene expression level was normalized by that of *gyrA* at days 1, 3 and 7 after infection of EA-hy296 cells. Data are shown as mean ± SD of triplicate measurements from two independent experiments. (ANOVA, n.s. : not statistically different; * $p<0.01$, ** $p<0.001$).

Figure 4. Carbon sources influence the transcription profile of the SigB pathway.

S. aureus USA300 WT strain was grown to stationary phase in CDM supplemented with glucose, ribose or fructose and gene expression profile of *rpiRc*, *sigB*, *rsbU, rsbW* and *asp23* was analysed by quantitative RT-PCR. Gene expression level was normalized by that of *gyrA*. Data are shown as mean ± SD of triplicate measurements from two independent experiments. Statistical significance was assessed in comparison to bacteria grown in CDM glucose (ANOVA, * $p<0.01$, ** $p<0.001$).

Figure 5. Bioavailability of PPP carbon sources impacts intracellular growth of *S. aureus*.

A. Intracellular proliferation of USA300 WT strain. Endothelial EA.Hy926 cells cultured in the presence of glucose, ribose or fructose and expressing a nuclear restricted Red Fluorescent Protein were infected with GFP expressing USA300 WT strains. One hour after infection cells were washed several times with gentamicin containing medium to eliminate extracellular bacteria. Gentamicin concentration of 50µg/ml was maintained throughout the experiment. Images were acquired every 30 minutes using Incucyte® S3 live cell imaging system. *Left panel.* Quantitative analysis representing the number of green particles divided by the number of red nuclei, during the first 24 hours after infection. Data are shown as mean ± SD of 6 replicates measurements. *Right panel*. Representative images (See also Video S4

and S5). Red: cell nuclei. Green: GFP expressing bacteria. For each line, a white circle was centred on a unique infected cell. Bar = 100µm.

B. Persistence of intracellular USA300 wild type strains. Endothelial EA.Hy926 cells cultured in no glucose DMEM supplemented with either glucose or ribose or fructose were infected with WT strain as described above. Gentamicin was maintained throughout the experiment. Survival of *S. aureus* was assessed by plating and counting CFUs the day of infection or three and seven days after infection. Results are shown as the average of $\log_{10}$ CFU/ml ± SD from three independent experiments (ANOVA, * $p<0.005$).

C. Transcription profile of intracellular *S. aureus*. One, three or seven days after infection cells were washed and collected. RNAs from intracellular *S. aureus* were prepared and gene expression of *sigB*, *rsbU, rsbW* and *asp23* was analysed by quantitative RT-PCR. Gene expression level was normalized by that of *gyrA*, at days 1, 3 and 7 after infection of EA-hy296 cells. Data are shown as mean ± SD of triplicate measurements from two independent experiments. (ANOVA, n.s. : not statistically different; * $p<0.05$; ** $p<0.005$).

Figure 6. Schematic depiction of the impact of TKT inactivation on *sigB* regulation.

A. SigB dependent regulation of *RNAIII* in WT context.

B. SigB dependent regulation of *RNAIII* in *Δtkt* context.

Legends of supplemental materials

Figure S1. Characterization of the *Δtkt* mutant strain.

A. Pentose Phosphate Pathway. Light blue: TKT enzymatic reaction.

B. Transketolase activity. Transketolase activity was monitored in USA300 WT, Δ*tkt* and Cp-*tkt*. Inactivation of *tkt* gene led to a significant decrease in TKT enzyme activity (ANOVA: * $p<0.001$).

C, D and E. Metabolomic analysis of the Δ*tkt* mutant strain.

Metabolomic analysis of the Δ*tkt* mutant strain. Quantitative metabolomic analysis was performed by ion chromatography and tandem mass spectrometry (IC-MS/MS) after BHI

overnight cultures from WT USA300 and Δ*tkt* mutant strains (see **Table S2**). **C**. Heatmap, obtained using MetaboAnalyst (https://www.metaboanalyst.ca), illustrate the metabolic shift between the two strains. **D and E**. Highlight on metabolic pathways. Light blue: TKT enzymatic reaction. Green arrow: increased concentration in Δ*tkt* mutant compared to WT strain. Red arrow: decreased concentration in Δ*tkt* mutant compared to WT strain.

Figure S2. Analysis of intracellular *S. aureus*

A. LAMP-1 colocalization assay. Endothelial EA.Hy926 cells were infected with GFP-expressing WT and Δ*tkt* mutant strains. One hour after infection, cells were washed several times with gentamicin containing medium to eliminate extracellular bacteria. A gentamicin concentration of 50µg/ml was maintained throughout the experiment. At 1 hour and 24 hours after infection cells were fixed using 4% PFA and processed for immunohistochemistry. Lysosomes were stained using anti-LAMP1 antibodies and images were acquired by confocal microscopy. Quantification of colocalization between GFP expressing USA300 WT or Δ*tkt* bacteria and LAMP-1 staining was obtained using ImageJ software. Data were obtained from more than 200 infected cells for each condition and expressed as % of bacteria associated with LAMP-1 ± SD. (ANOVA; n.s.: not statistically different; * $p<0.05$).

B. Transcription profile of intracellular *S. aureus*.

Endothelial EA.Hy926 cells were infected with Δ*tkt* and Δ*hemDBL* mutant strains as described in figure 2. One, three or seven days after infection cells were washed and collected. RNA from intracellular *S. aureus* were prepared and gene expression of *RNAIII*, *rpiRc*, *sigB*, *rsbU, rsbW* and *asp23* was analysed by quantitative RT-PCR. Gene expression level was normalized by that of *gyrA* at days 1, 3 and 7 after infection of EA-hy296 cells. Data obtained for Δ*tkt* mutant strain was the same as those showed in figure 3. Data obtained from Δ*hemDBL* mutant strain are shown as mean ± SD of a triplicate measurements (ANOVA, * $p<0.01$, ** $p<0.001$).

Figure S3. Metabolomic analysis of endothelial cells grown in no glucose DMEM supplemented with glucose, fructose or ribose (raw data are presented in Table S2).

A. Growth of USA300 WT strain in chemically defined medium (CDM) supplemented with glucose or fructose and incubated 21h at 37°C. Optic densities were measured every-hour from 0 to 8 hours and then at 21 hours. Curve is a representative experiment.

B. Metabolomic analysis of endothelial cells grown in no glucose DMEM supplemented with glucose, fructose or ribose (raw data are presented in Table S2). Semi-quantitative metabolomic analysis was performed by ion chromatography and tandem mass spectrometry after 1, 3 or 7 day(s) culture in DMEM with 25 mM glucose, fructose or ribose. n.d.: not detected. Data are expressed as area under the curve (Arbitrary Units ± SEM).

Movie S1: Intracellular proliferation of USA300 wild type strain. Endothelial EA.Hy926 cells expressing a nuclear restricted Red Fluorescent Protein were infected with GFP expressing wild type strains. One hour after infection cells were washed several times with gentamicin containing medium to eliminate extracellular bacteria (see materials and methods section). Gentamicin concentration of 50µg/ml was maintained throughout the experiment. Images were acquired every 30 minutes using Incucyte® S3 live cell imaging system.

Movie S2: Intracellular proliferation of USA300 Δ*tkt* mutant strain. Same protocol as above in movie S1.

Movie S3: Intracellular proliferation of USA300 Δ*hemDBL* mutant strain. Same protocol as above in movie S1.

Movie S4: Intracellular proliferation of USA300 wild type strain. Cells were grown in no glucose DMEM supplemented with fructose**.** Same protocol as above in movie S1**.**

Movie S5: Intracellular proliferation of USA300 wild type strain. Cells were grown in no glucose DMEM supplemented with ribose**.** Same protocol as above in movie S1**.**

References

1. **Otto M.** 2013. Community-associated MRSA: what makes them special? Int J Med Microbiol **303:**324-330.
2. **Thomer L, Schneewind O, Missiakas D.** 2016. Pathogenesis of Staphylococcus aureus Bloodstream Infections. Annual review of pathology **11:**343-364.
3. **Strauss L, Stegger M, Akpaka PE, Alabi A, Breurec S, Coombs G, Egyir B, Larsen AR, Laurent F, Monecke S, Peters G, Skov R, Strommenger B, Vandenesch F, Schaumburg F, Mellmann A.** 2017. Origin, evolution, and global transmission of community-acquired Staphylococcus aureus ST8. Proceedings of the National Academy of Sciences of the United States of America **114:**E10596-E10604.
4. **DeLeo FR, Otto M, Kreiswirth BN, Chambers HF.** 2010. Community-associated meticillin-resistant Staphylococcus aureus. Lancet **375:**1557-1568.
5. **Nimmo GR.** 2012. USA300 abroad: global spread of a virulent strain of community-associated methicillin-resistant Staphylococcus aureus. Clin Microbiol Infect **18:**725-734.
6. **Fisher RA, Gollan B, Helaine S.** 2017. Persistent bacterial infections and persister cells. Nature reviews. Microbiology **15:**453-464.
7. **Tuchscherr L, Bischoff M, Lattar SM, Noto Llana M, Pfortner H, Niemann S, Geraci J, Van de Vyver H, Fraunholz MJ, Cheung AL, Herrmann M, Volker U, Sordelli DO, Peters G, Loffler B.** 2015. Sigma Factor SigB Is Crucial to Mediate Staphylococcus aureus Adaptation during Chronic Infections. PLoS pathogens **11:**e1004870.
8. **Conlon BP, Rowe SE, Gandt AB, Nuxoll AS, Donegan NP, Zalis EA, Clair G, Adkins JN, Cheung AL, Lewis K.** 2016. Persister formation in Staphylococcus aureus is associated with ATP depletion. Nature microbiology **1**.
9. **Proctor RA, von Eiff C, Kahl BC, Becker K, McNamara P, Herrmann M, Peters G.** 2006. Small colony variants: a pathogenic form of bacteria that facilitates persistent and recurrent infections. Nature reviews. Microbiology **4:**295-305.

10. **Tuchscherr L, Heitmann V, Hussain M, Viemann D, Roth J, von Eiff C, Peters G, Becker K, Loffler B.** 2010. Staphylococcus aureus small-colony variants are adapted phenotypes for intracellular persistence. The Journal of infectious diseases **202:**1031-1040.

11. **Tuchscherr L, Kreis CA, Hoerr V, Flint L, Hachmeister M, Geraci J, Bremer-Streck S, Kiehntopf M, Medina E, Kribus M, Raschke M, Pletz M, Peters G, Loffler B.** 2016. Staphylococcus aureus develops increased resistance to antibiotics by forming dynamic small colony variants during chronic osteomyelitis. The Journal of antimicrobial chemotherapy **71:**438-448.

12. **Sadowska B, Bonar A, von Eiff C, Proctor RA, Chmiela M, Rudnicka W, Rozalska B.** 2002. Characteristics of Staphylococcus aureus, isolated from airways of cystic fibrosis patients, and their small colony variants. FEMS immunology and medical microbiology **32:**191-197.

13. **Chatterjee I, Kriegeskorte A, Fischer A, Deiwick S, Theimann N, Proctor RA, Peters G, Herrmann M, Kahl BC.** 2008. In vivo mutations of thymidylate synthase (encoded by thyA) are responsible for thymidine dependency in clinical small-colony variants of Staphylococcus aureus. Journal of bacteriology **190:**834-842.

14. **Kohler C, von Eiff C, Peters G, Proctor RA, Hecker M, Engelmann S.** 2003. Physiological characterization of a heme-deficient mutant of Staphylococcus aureus by a proteomic approach. Journal of bacteriology **185:**6928-6937.

15. **Kohler C, von Eiff C, Liebeke M, McNamara PJ, Lalk M, Proctor RA, Hecker M, Engelmann S.** 2008. A defect in menadione biosynthesis induces global changes in gene expression in Staphylococcus aureus. Journal of bacteriology **190:**6351-6364.

16. **von Eiff C, Heilmann C, Proctor RA, Woltz C, Peters G, Gotz F.** 1997. A site-directed Staphylococcus aureus hemB mutant is a small-colony variant which persists intracellularly. Journal of bacteriology **179:**4706-4712.

17. **Kalinka J, Hachmeister M, Geraci J, Sordelli D, Hansen U, Niemann S, Oetermann S, Peters G, Loffler B, Tuchscherr L.** 2014. Staphylococcus aureus isolates from chronic osteomyelitis are characterized by high host cell invasion and

intracellular adaptation, but still induce inflammation. Int J Med Microbiol **304:**1038-1049.

18. **Rollin G, Tan X, Tros F, Dupuis M, Nassif X, Charbit A, Coureuil M.** 2017. Intracellular Survival of Staphylococcus aureus in Endothelial Cells: A Matter of Growth or Persistence. Frontiers in microbiology **8:**1354.

19. **TAN X, Coureuil M, Ramond E, Euphrasie D, Dupuis M, Tros F, Meyer J, Nemanzny I, Chhuon C, Guerrera IC, Ferroni A, Sermet-Gaudelus I, Nassif X, Charbit A, Jamet A.** 2018. Chronic Staphylococcus aureus lung infection correlates with proteogenomic and metabolic adaptations leading to an increased intracellular persistence. bioRxiv.

20. **Strobel M, Pfortner H, Tuchscherr L, Volker U, Schmidt F, Kramko N, Schnittler HJ, Fraunholz MJ, Loffler B, Peters G, Niemann S.** 2016. Post-invasion events after infection with Staphylococcus aureus are strongly dependent on both the host cell type and the infecting S. aureus strain. Clin Microbiol Infect **22:**799-809.

21. **Hayes SM, Howlin R, Johnston DA, Webb JS, Clarke SC, Stoodley P, Harries PG, Wilson SJ, Pender SL, Faust SN, Hall-Stoodley L, Salib RJ.** 2015. Intracellular residency of Staphylococcus aureus within mast cells in nasal polyps: A novel observation. The Journal of allergy and clinical immunology **135:**1648-1651.

22. **Ou J, Drilling A, Singhal D, Tan NC, Wallis-Hill D, Vreugde S, Psaltis AJ, Wormald PJ.** 2016. Association of intracellular Staphylococcus aureus with prognosis in chronic rhinosinusitis. International forum of allergy & rhinology **6:**792-799.

23. **Hanssen AM, Kindlund B, Stenklev NC, Furberg AS, Fismen S, Olsen RS, Johannessen M, Sollid JU.** 2017. Localization of Staphylococcus aureus in tissue from the nasal vestibule in healthy carriers. BMC microbiology **17:**89.

24. **Moldovan A, Fraunholz MJ.** 2018. In or out: phagosomal escape of Staphylococcus aureus. Cellular microbiology**:**e12997.

25. **Branger C, Gardye C, Lambert-Zechovsky N.** 1996. Persistence of Staphylococcus aureus strains among cystic fibrosis patients over extended periods of time. J Med Microbiol **45:**294-301.

26. **Kahl BC, Duebbers A, Lubritz G, Haeberle J, Koch HG, Ritzerfeld B, Reilly M, Harms E, Proctor RA, Herrmann M, Peters G.** 2003. Population dynamics of persistent Staphylococcus aureus isolated from the airways of cystic fibrosis patients during a 6-year prospective study. Journal of clinical microbiology **41:**4424-4427.

27. **Grosz M, Kolter J, Paprotka K, Winkler AC, Schafer D, Chatterjee SS, Geiger T, Wolz C, Ohlsen K, Otto M, Rudel T, Sinha B, Fraunholz M.** 2014. Cytoplasmic replication of Staphylococcus aureus upon phagosomal escape triggered by phenol-soluble modulin alpha. Cellular microbiology **16:**451-465.

28. **Korea CG, Balsamo G, Pezzicoli A, Merakou C, Tavarini S, Bagnoli F, Serruto D, Unnikrishnan M.** 2014. Staphylococcal Esx proteins modulate apoptosis and release of intracellular Staphylococcus aureus during infection in epithelial cells. Infection and immunity **82:**4144-4153.

29. **Kriegeskorte A, Konig S, Sander G, Pirkl A, Mahabir E, Proctor RA, von Eiff C, Peters G, Becker K.** 2011. Small colony variants of Staphylococcus aureus reveal distinct protein profiles. Proteomics **11:**2476-2490.

30. **Kriegeskorte A, Grubmuller S, Huber C, Kahl BC, von Eiff C, Proctor RA, Peters G, Eisenreich W, Becker K.** 2014. Staphylococcus aureus small colony variants show common metabolic features in central metabolism irrespective of the underlying auxotrophism. Frontiers in cellular and infection microbiology **4:**141.

31. **Tuchscherr L, Loffler B.** 2016. Staphylococcus aureus dynamically adapts global regulators and virulence factor expression in the course from acute to chronic infection. Current genetics **62:**15-17.

32. **Stincone A, Prigione A, Cramer T, Wamelink MM, Campbell K, Cheung E, Olin-Sandoval V, Gruning NM, Kruger A, Tauqeer Alam M, Keller MA, Breitenbach M, Brindle KM, Rabinowitz JD, Ralser M.** 2015. The return of metabolism:

biochemistry and physiology of the pentose phosphate pathway. Biological reviews of the Cambridge Philosophical Society **90:**927-963.

33. **Harper L, Balasubramanian D, Ohneck EA, Sause WE, Chapman J, Mejia-Sosa B, Lhakhang T, Heguy A, Tsirigos A, Ueberheide B, Boyd JM, Lun DS, Torres VJ.** 2018. Staphylococcus aureus Responds to the Central Metabolite Pyruvate To Regulate Virulence. mBio **9**.

34. **Purves J, Cockayne A, Moody PC, Morrissey JA.** 2010. Comparison of the regulation, metabolic functions, and roles in virulence of the glyceraldehyde-3-phosphate dehydrogenase homologues gapA and gapB in Staphylococcus aureus. Infection and immunity **78:**5223-5232.

35. **Vitko NP, Spahich NA, Richardson AR.** 2015. Glycolytic dependency of high-level nitric oxide resistance and virulence in Staphylococcus aureus. mBio **6**.

36. **Vitko NP, Grosser MR, Khatri D, Lance TR, Richardson AR.** 2016. Expanded Glucose Import Capability Affords Staphylococcus aureus Optimized Glycolytic Flux during Infection. mBio **7**.

37. **Gardner SG, Marshall DD, Daum RS, Powers R, Somerville GA.** 2018. Metabolic Mitigation of Staphylococcus aureus Vancomycin Intermediate-Level Susceptibility. Antimicrobial agents and chemotherapy **62**.

38. **Fleury B, Kelley WL, Lew D, Gotz F, Proctor RA, Vaudaux P.** 2009. Transcriptomic and metabolic responses of Staphylococcus aureus exposed to supra-physiological temperatures. BMC microbiology **9:**76.

39. **Joseph B, Schneiker-Bekel S, Schramm-Gluck A, Blom J, Claus H, Linke B, Schwarz RF, Becker A, Goesmann A, Frosch M, Schoen C.** 2010. Comparative genome biology of a serogroup B carriage and disease strain supports a polygenic nature of meningococcal virulence. Journal of bacteriology **192:**5363-5377.

40. **Mekonnen SA, Palma Medina LM, Michalik S, Loreti MG, Gesell Salazar M, van Dijl JM, Volker U.** 2018. Metabolic niche adaptation of community- and hospital-associated methicillin-resistant Staphylococcus aureus. Journal of proteomics.

41. **Zhu Y, Nandakumar R, Sadykov MR, Madayiputhiya N, Luong TT, Gaupp R, Lee CY, Somerville GA.** 2011. RpiR homologues may link Staphylococcus aureus RNAIII synthesis and pentose phosphate pathway regulation. Journal of bacteriology **193:**6187-6196.

42. **Gaupp R, Wirf J, Wonnenberg B, Biegel T, Eisenbeis J, Graham J, Herrmann M, Lee CY, Beisswenger C, Wolz C, Tschernig T, Bischoff M, Somerville GA.** 2016. RpiRc Is a Pleiotropic Effector of Virulence Determinant Synthesis and Attenuates Pathogenicity in Staphylococcus aureus. Infection and immunity **84:**2031-2041.

43. **Balasubramanian D, Ohneck EA, Chapman J, Weiss A, Kim MK, Reyes-Robles T, Zhong J, Shaw LN, Lun DS, Ueberheide B, Shopsin B, Torres VJ.** 2016. Staphylococcus aureus Coordinates Leukocidin Expression and Pathogenesis by Sensing Metabolic Fluxes via RpiRc. mBio **7**.

44. **Sprenger GA, Schorken U, Sprenger G, Sahm H.** 1995. Transketolase A of Escherichia coli K12. Purification and properties of the enzyme from recombinant strains. Eur J Biochem **230:**525-532.

45. **Fullam E, Pojer F, Bergfors T, Jones TA, Cole ST.** 2012. Structure and function of the transketolase from Mycobacterium tuberculosis and comparison with the human enzyme. Open biology **2:**110026.

46. **Hussain M, Hastings JG, White PJ.** 1991. A chemically defined medium for slime production by coagulase-negative staphylococci. J Med Microbiol **34:**143-147.

47. **Boisset S, Geissmann T, Huntzinger E, Fechter P, Bendridi N, Possedko M, Chevalier C, Helfer AC, Benito Y, Jacquier A, Gaspin C, Vandenesch F, Romby P.** 2007. Staphylococcus aureus RNAIII coordinately represses the synthesis of virulence factors and the transcription regulator Rot by an antisense mechanism. Genes & development **21:**1353-1366.

48. **Mader U, Nicolas P, Depke M, Pane-Farre J, Debarbouille M, van der Kooi-Pol MM, Guerin C, Derozier S, Hiron A, Jarmer H, Leduc A, Michalik S, Reilman E, Schaffer M, Schmidt F, Bessieres P, Noirot P, Hecker M, Msadek T, Volker U,**

van Dijl JM. 2016. Staphylococcus aureus Transcriptome Architecture: From Laboratory to Infection-Mimicking Conditions. PLoS genetics **12:**e1005962.

49. **Mitchell G, Fugere A, Pepin Gaudreau K, Brouillette E, Frost EH, Cantin AM, Malouin F.** 2013. SigB is a dominant regulator of virulence in Staphylococcus aureus small-colony variants. PloS one **8:**e65018.

50. **Pane-Farre J, Jonas B, Hardwick SW, Gronau K, Lewis RJ, Hecker M, Engelmann S.** 2009. Role of RsbU in controlling SigB activity in Staphylococcus aureus following alkaline stress. Journal of bacteriology **191:**2561-2573.

51. **Gertz S, Engelmann S, Schmid R, Ohlsen K, Hacker J, Hecker M.** 1999. Regulation of sigmaB-dependent transcription of sigB and asp23 in two different Staphylococcus aureus strains. Molecular & general genetics : MGG **261:**558-566.

52. **Kupferwasser LI, Yeaman MR, Nast CC, Kupferwasser D, Xiong YQ, Palma M, Cheung AL, Bayer AS.** 2003. Salicylic acid attenuates virulence in endovascular infections by targeting global regulatory pathways in Staphylococcus aureus. The Journal of clinical investigation **112:**222-233.

53. **Garzoni C, Kelley WL.** 2009. Staphylococcus aureus: new evidence for intracellular persistence. Trends in microbiology **17:**59-65.

54. **Mitchell G, Gattuso M, Grondin G, Marsault E, Bouarab K, Malouin F.** 2011. Tomatidine inhibits replication of Staphylococcus aureus small-colony variants in cystic fibrosis airway epithelial cells. Antimicrobial agents and chemotherapy **55:**1937-1945.

55. **Sendi P, Proctor RA.** 2009. Staphylococcus aureus as an intracellular pathogen: the role of small colony variants. Trends in microbiology **17:**54-58.

56. **Tuchscherr L, Medina E, Hussain M, Volker W, Heitmann V, Niemann S, Holzinger D, Roth J, Proctor RA, Becker K, Peters G, Loffler B.** 2011. Staphylococcus aureus phenotype switching: an effective bacterial strategy to escape host immune response and establish a chronic infection. EMBO molecular medicine **3:**129-141.

57. **Roux A, Todd DA, Velazquez JV, Cech NB, Sonenshein AL.** 2014. CodY-mediated regulation of the Staphylococcus aureus Agr system integrates nutritional and population density signals. Journal of bacteriology **196:**1184-1196.

58. **Romilly C, Lays C, Tomasini A, Caldelari I, Benito Y, Hammann P, Geissmann T, Boisset S, Romby P, Vandenesch F.** 2014. A non-coding RNA promotes bacterial persistence and decreases virulence by regulating a regulator in Staphylococcus aureus. PLoS pathogens **10:**e1003979.

59. **Felden B, Vandenesch F, Bouloc P, Romby P.** 2011. The Staphylococcus aureus RNome and its commitment to virulence. PLoS pathogens **7:**e1002006.

60. **Seggewiss J, Becker K, Kotte O, Eisenacher M, Yazdi MR, Fischer A, McNamara P, Al Laham N, Proctor R, Peters G, Heinemann M, von Eiff C.** 2006. Reporter metabolite analysis of transcriptional profiles of a Staphylococcus aureus strain with normal phenotype and its isogenic hemB mutant displaying the small-colony-variant phenotype. Journal of bacteriology **188:**7765-7777.

61. **von Eiff C, McNamara P, Becker K, Bates D, Lei XH, Ziman M, Bochner BR, Peters G, Proctor RA.** 2006. Phenotype microarray profiling of Staphylococcus aureus menD and hemB mutants with the small-colony-variant phenotype. Journal of bacteriology **188:**687-693.

62. **Somerville GA, Cockayne A, Durr M, Peschel A, Otto M, Musser JM.** 2003. Synthesis and deformylation of Staphylococcus aureus delta-toxin are linked to tricarboxylic acid cycle activity. Journal of bacteriology **185:**6686-6694.

63. **Somerville GA, Chaussee MS, Morgan CI, Fitzgerald JR, Dorward DW, Reitzer LJ, Musser JM.** 2002. Staphylococcus aureus aconitase inactivation unexpectedly inhibits post-exponential-phase growth and enhances stationary-phase survival. Infection and immunity **70:**6373-6382.

64. **Ding Y, Liu X, Chen F, Di H, Xu B, Zhou L, Deng X, Wu M, Yang CG, Lan L.** 2014. Metabolic sensor governing bacterial virulence in Staphylococcus aureus. Proceedings of the National Academy of Sciences of the United States of America **111:**E4981-4990.

65. **Zhang DM, Jiao RQ, Kong LD.** 2017. High Dietary Fructose: Direct or Indirect Dangerous Factors Disturbing Tissue and Organ Functions. Nutrients **9**.

66. **Glushakova O, Kosugi T, Roncal C, Mu W, Heinig M, Cirillo P, Sanchez-Lozada LG, Johnson RJ, Nakagawa T.** 2008. Fructose induces the inflammatory molecule ICAM-1 in endothelial cells. Journal of the American Society of Nephrology : JASN **19:**1712-1720.

67. **Gross M, Zollner N.** 1991. Serum levels of glucose, insulin, and C-peptide during long-term D-ribose administration in man. Klinische Wochenschrift **69:**31-36.

68. **Pilz RB, Willis RC, Boss GR.** 1984. The influence of ribose 5-phosphate availability on purine synthesis of cultured human lymphoblasts and mitogen-stimulated lymphocytes. The Journal of biological chemistry **259:**2927-2935.

69. **Lei MG, Lee CY.** 2015. RbsR Activates Capsule but Represses the rbsUDK Operon in Staphylococcus aureus. Journal of bacteriology **197:**3666-3675.

70. **Arnaud M, Chastanet A, Debarbouille M.** 2004. New vector for efficient allelic replacement in naturally nontransformable, low-GC-content, gram-positive bacteria. Applied and environmental microbiology **70:**6887-6891.

71. **Jacobus AP, Gross J.** 2015. Optimal cloning of PCR fragments by homologous recombination in Escherichia coli. PloS one **10:**e0119221.

72. **Garzoni C, Francois P, Huyghe A, Couzinet S, Tapparel C, Charbonnier Y, Renzoni A, Lucchini S, Lew DP, Vaudaux P, Kelley WL, Schrenzel J.** 2007. A global view of Staphylococcus aureus whole genome expression upon internalization in human epithelial cells. BMC genomics **8:**171.

73. **Mackay GM, Zheng L, van den Broek NJ, Gottlieb E.** 2015. Analysis of Cell Metabolism Using LC-MS and Isotope Tracers. Methods in enzymology **561:**171-196.

74. **Chong J, Soufan O, Li C, Caraus I, Li S, Bourque G, Wishart DS, Xia J.** 2018. MetaboAnalyst 4.0: towards more transparent and integrative metabolomics analysis. Nucleic acids research **46:**W486-W494.

75. **Xia J, Wishart DS.** 2016. Using MetaboAnalyst 3.0 for Comprehensive Metabolomics Data Analysis. Current protocols in bioinformatics **55:**14 10 11-14 10 91.

76. **Shaw JA, Henard CA, Liu L, Dieckman LM, Vazquez-Torres A, Bourret TJ.** 2018. Salmonella enterica serovar Typhimurium has three transketolase enzymes contributing to the pentose phosphate pathway. The Journal of biological chemistry **293:**11271-11282.

Figure 1

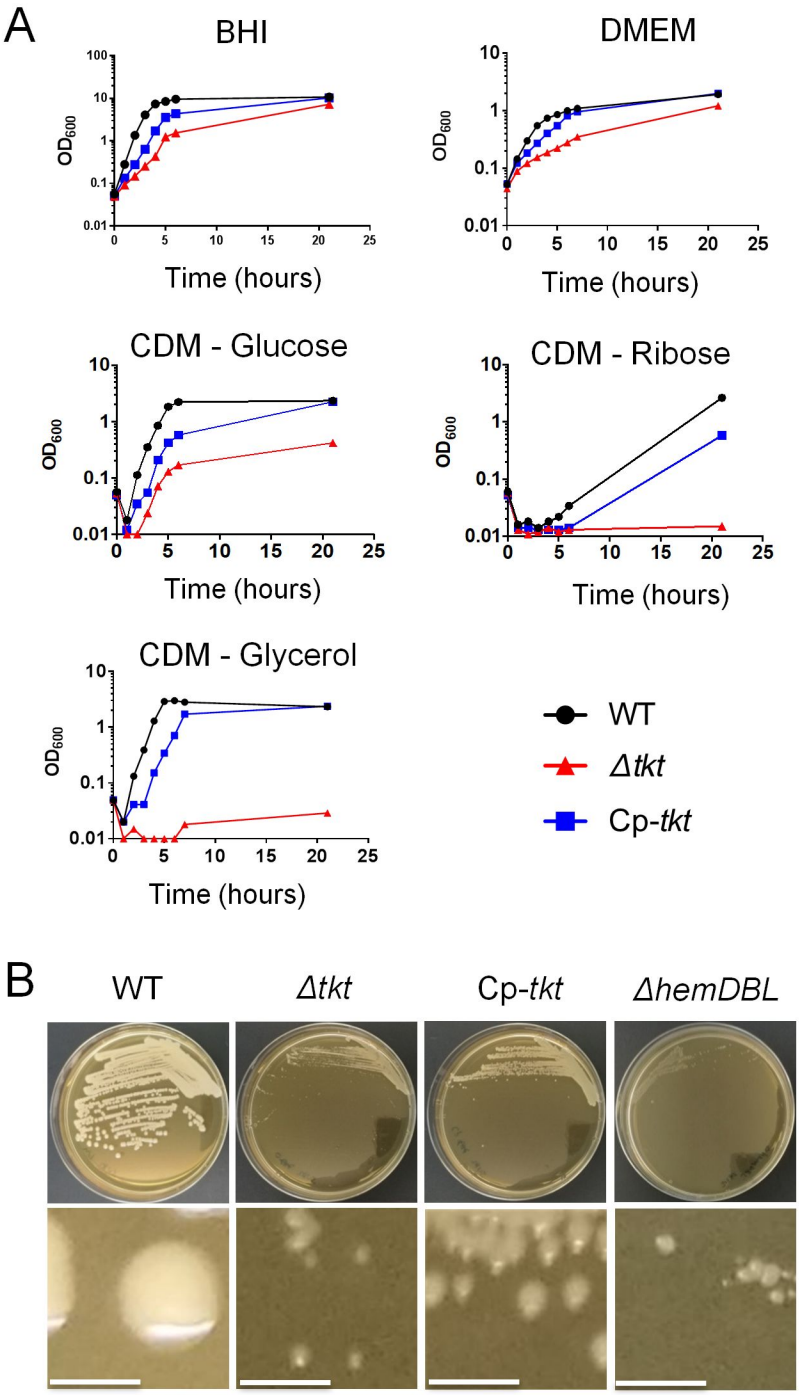
A
BHI
DMEM
CDM - Glucose
CDM - Ribose
CDM - Glycerol
OD600
Time (hours)
WT
Δtkt
Cp-tkt
B
WT
Δtkt
Cp-tkt
ΔhemDBL

Figure 2

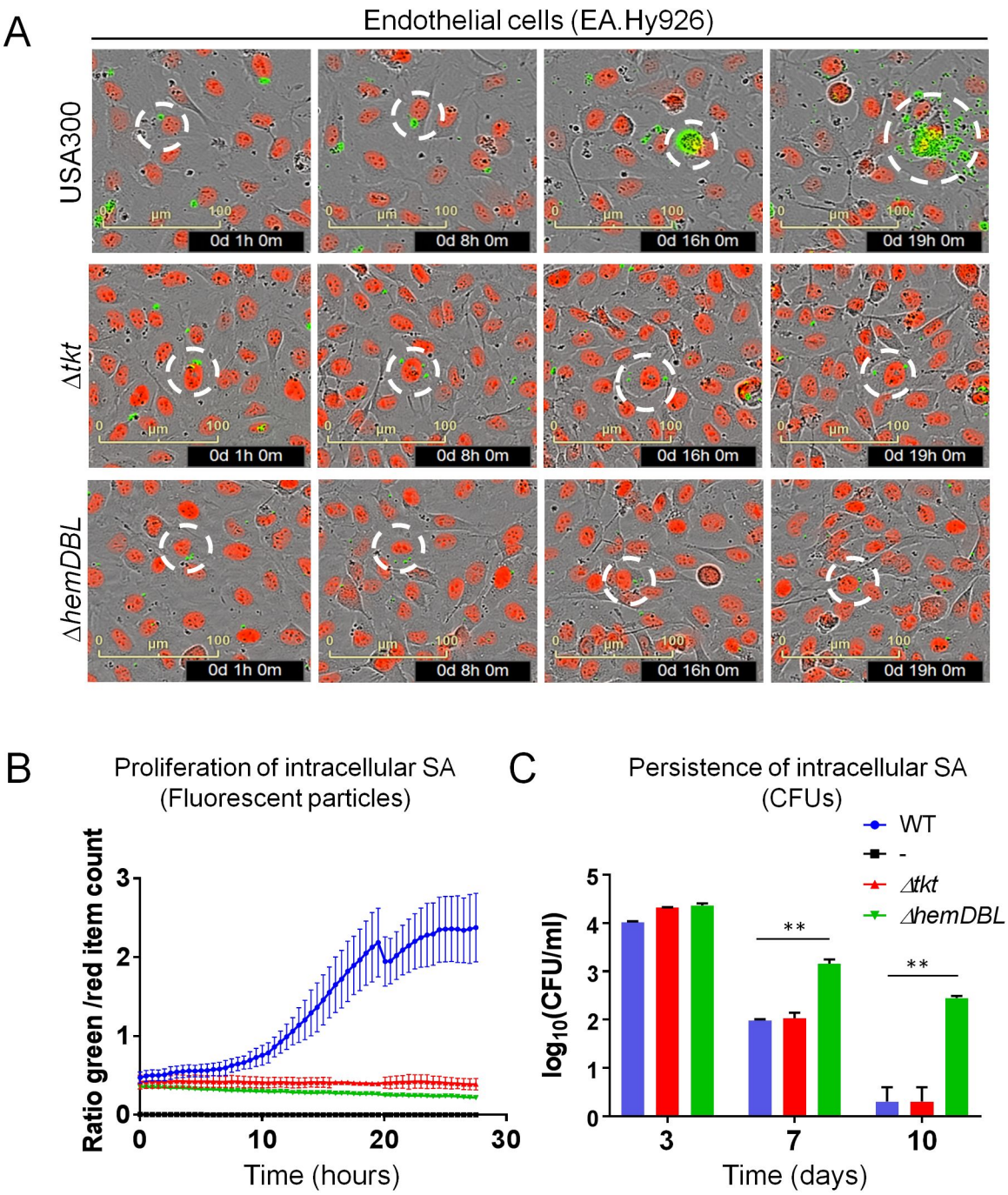
A
Endothelial cells (EA.Hy926)
USA300
Δtkt
ΔhemDBL
0d 1h 0m
0d 8h 0m
0d 16h 0m
0d 19h 0m
B
Proliferation of intracellular SA
(Fluorescent particles)
Ratio green /red item count
Time (hours)
C
Persistence of intracellular SA
(CFUs)
WT
-
Δtkt
ΔhemDBL
log10(CFU/ml)
Time (days)
**
**

Figure 3

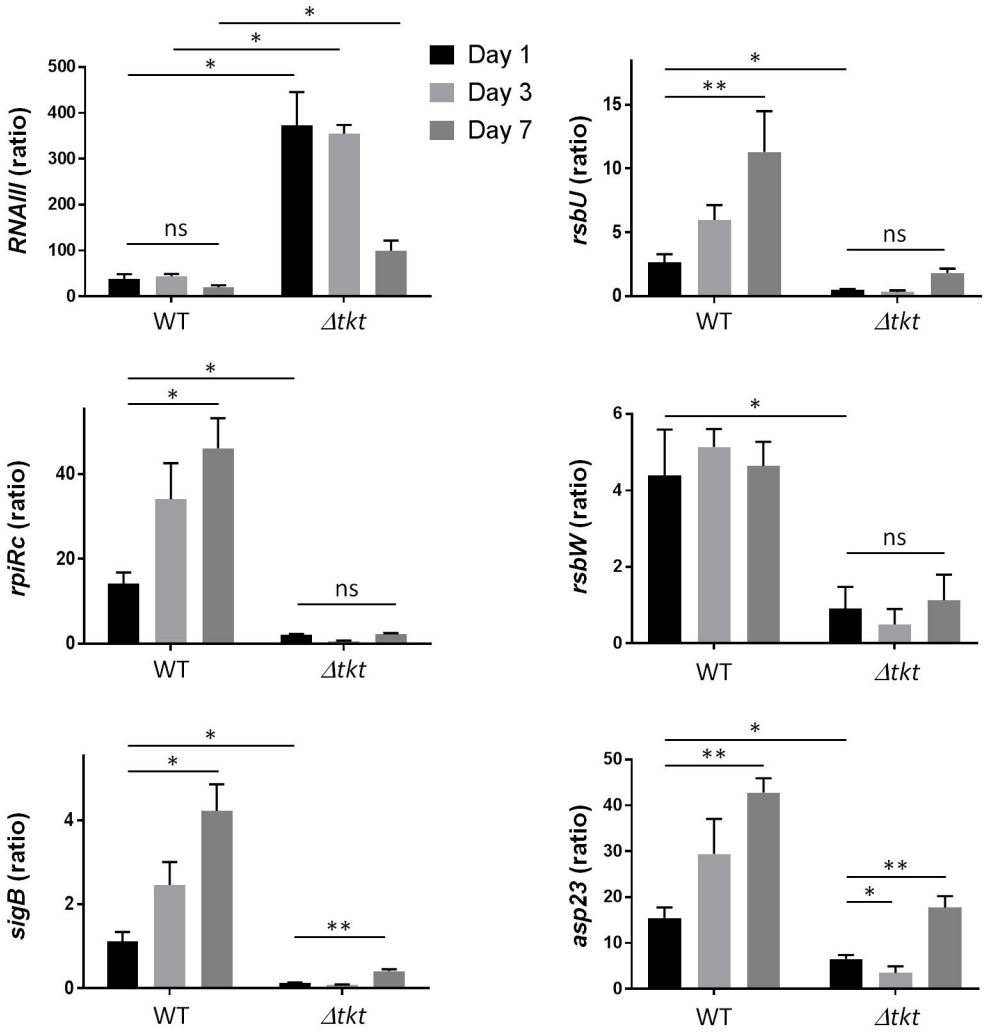
Day 1
Day 3
Day 7
RNAIII (ratio)
rsbU (ratio)
rpiRc (ratio)
rsbW (ratio)
sigB (ratio)
asp23 (ratio)
WT
Δtkt
ns
*
**

Figure 4

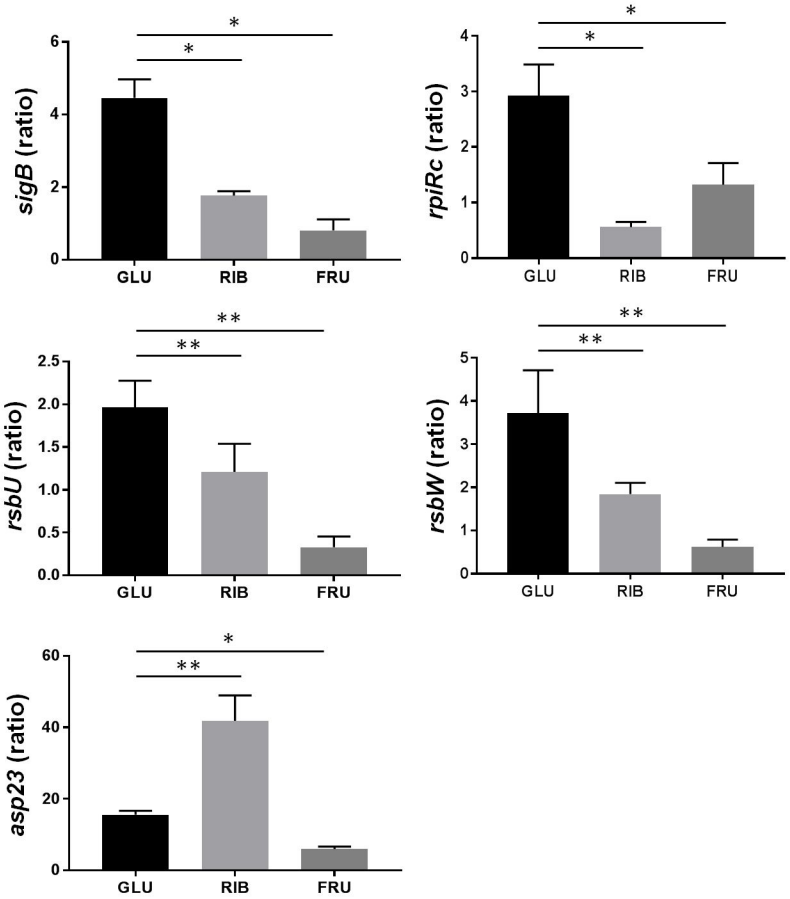
*
*
sigB (ratio)
6
4
2
0
GLU
RIB
FRU
*
*
rpiRc (ratio)
4
3
2
1
0
GLU
RIB
FRU
**
**
rsbU (ratio)
2.5
2.0
1.5
1.0
0.5
0.0
GLU
RIB
FRU
**
**
rsbW (ratio)
5
4
3
2
1
0
GLU
RIB
FRU
*
**
asp23 (ratio)
60
40
20
0
GLU
RIB
FRU

Figure 5

A

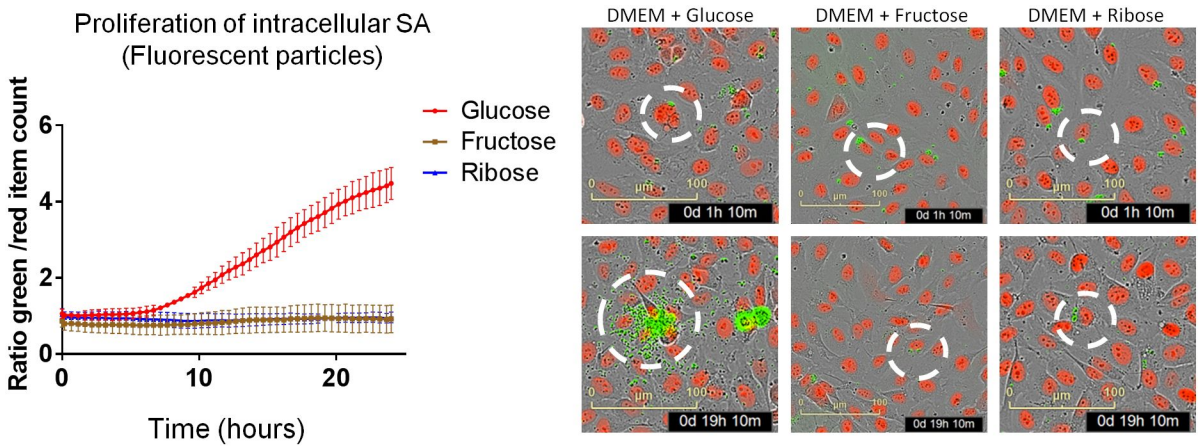
Proliferation of intracellular SA
(Fluorescent particles)
Ratio green /red item count
Time (hours)
Glucose
Fructose
Ribose
DMEM + Glucose
DMEM + Fructose
DMEM + Ribose
0d 1h 10m
0d 19h 10m

B

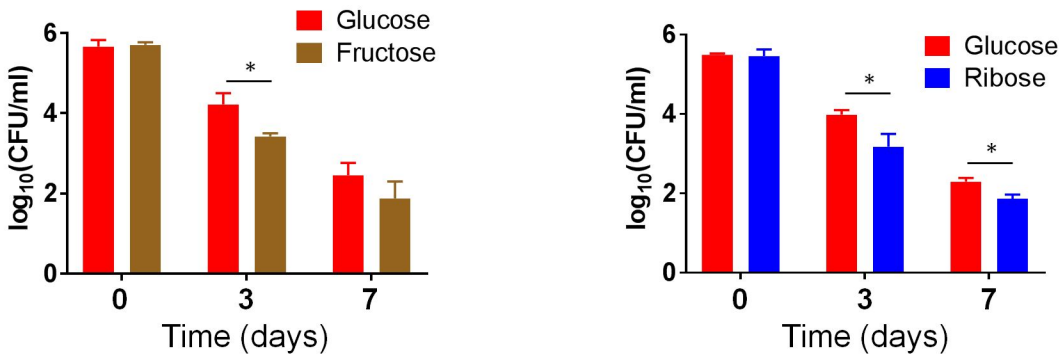
Glucose
Fructose
Ribose
log10(CFU/ml)
Time (days)

C

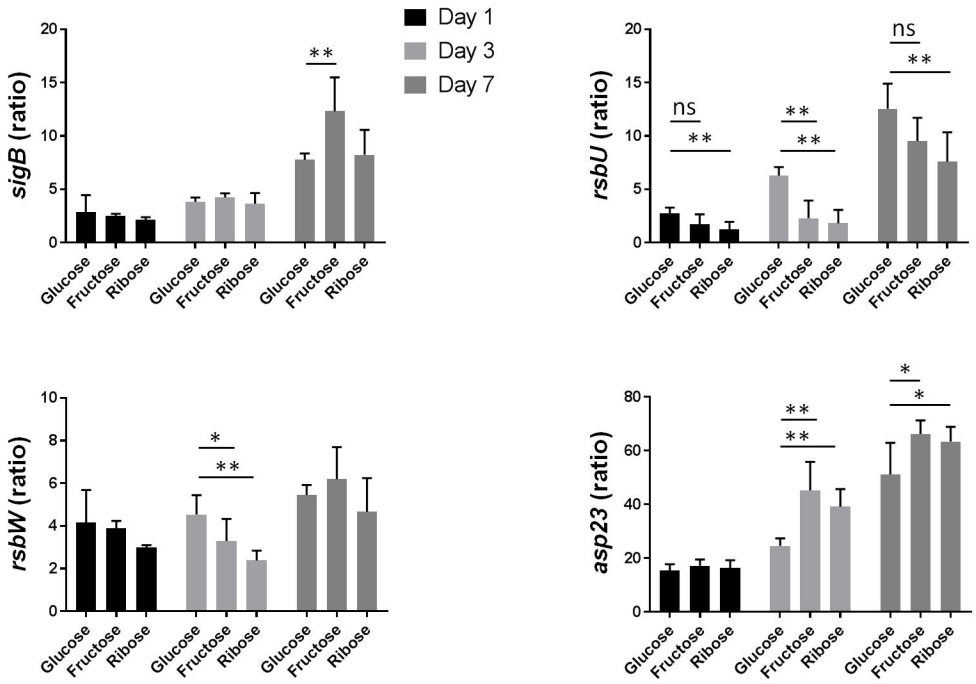
Day 1
Day 3
Day 7
sigB (ratio)
rsbU (ratio)
rsbW (ratio)
asp23 (ratio)
Glucose
Fructose
Ribose
ns

Figure 6

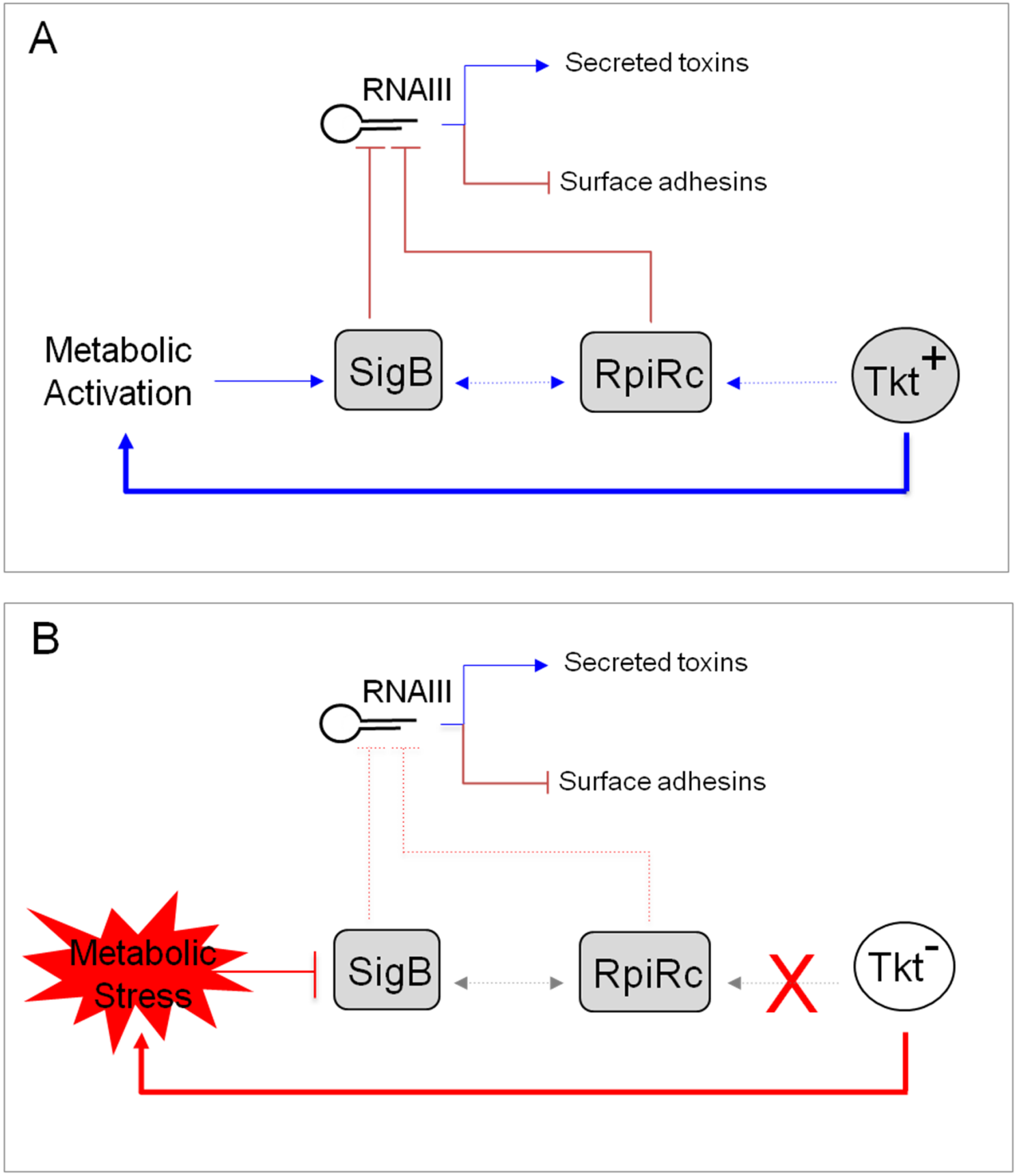
A
RNAIII
Secreted toxins
Surface adhesins
Metabolic Activation
SigB
RpiRc
Tkt+
B
RNAIII
Secreted toxins
Surface adhesins
Metabolic Stress
SigB
RpiRc
X
Tkt-